

Spin-orbit Energies in Etch-Confined Superconductor-Semiconductor Nanowires

J. D. S. Witt,^{1,*} G. C. Gardner,^{2,3} C. Thomas,^{2,3} T. Lindemann,^{2,3}
S. Gronin,^{2,3} M. J. Manfra,^{2,3} and D. J. Reilly^{1,4,†}

¹*ARC Centre of Excellence for Engineered Quantum Systems,*

School of Physics, The University of Sydney, Sydney, NSW 2006, Australia

²*Department of Physics and Astronomy, Purdue University, West Lafayette, Indiana, USA*

³*Microsoft Quantum Purdue, Purdue University, West Lafayette, Indiana, USA*

⁴*Microsoft Quantum Sydney, The University of Sydney, Sydney, NSW 2006, Australia*

(Dated: November 25, 2021)

We report magneto-transport measurements of quasi-1-dimensional (1D) Al-InAs nanowires produced via etching of a hybrid superconductor-semiconductor two-dimensional electron gas (2DEG). Tunnel spectroscopy measurements above the superconducting gap provide a means of identifying the 1D sub-bands associated with the confined 1D region. Fitting the data reveals the strength of the different components of the spin-orbit interaction (SOI), which is of interest for evaluating the suitability of superconductor-semiconductor 2DEGs for realizing Majorana qubits.

I. INTRODUCTION

Hybrid superconductor-semiconductor devices theoretically provide all of the requisite ingredients to generate Majorana quasiparticles. The combination of s -wave pairing, strong spin-orbit interaction (SOI), and gate-control over the chemical potential enables the engineering of an effective spinless, p -wave, superconducting topological phase. This phase has a multiply degenerate ground state, the edge-states of which are zero-energy modes or Majorana bound states (MBS) – so-called because they are the quasiparticle analogue of the theoretical Majorana fermion. By virtue of being their own antiparticle, MBS are incapable of coexisting in the same physical space. Thereby, an additional requirement for MBS generation is that the proposed host system possesses an odd number of conduction modes [1, 2].

To-date, experimental efforts to engineer systems capable of hosting MBS have followed three key routes: Vapour-liquid-solid (VLS) nanowires [3–10]; selective-area growth (SAG) molecular beam epitaxy [11–16]; and heterostructures supporting 2DEGs, where subtractive etching of material or gate-based depletion is used to define 1D regions [17–20]. VLS nanowires have received much focus, but scale-up of this platform into the complex arrays needed for quantum computing is challenging [21, 22]. The alternate approaches perhaps offer more feasible routes for fabricating scalable qubit arrays. The opportunity to suppress disorder by using 2D heterostructures with super-lattice buffers [23, 24] whilst retaining the flexibility of patterning needed for scaling-up provides further motivation for studying 2DEGs. However, despite their promise, open questions remain concerning the extent to which the favourable properties of 2DEG based systems remain when 1D regions are defined using etching or gate-depletion.

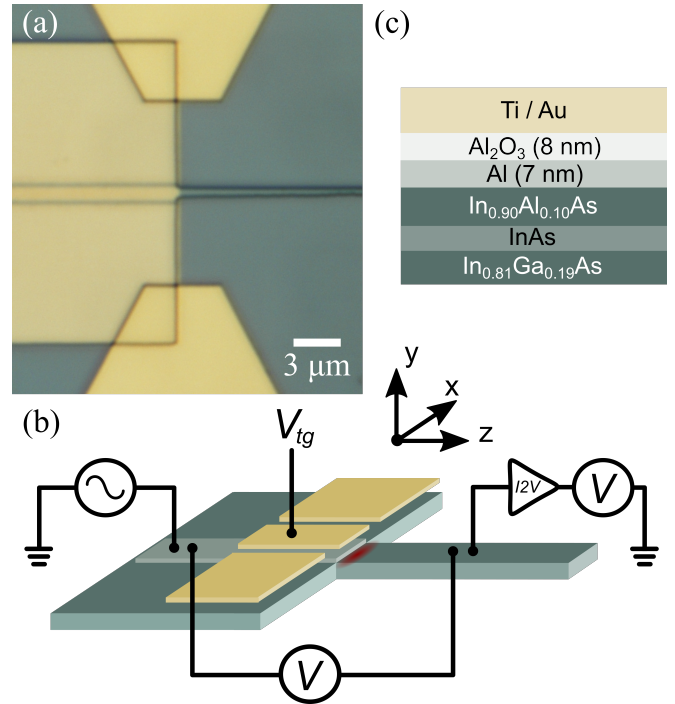


FIG. 1. (a) Device micrograph, (b) device schematic indicating the measurement set-up – 4-point measurements were made by contacting the aluminium strip on the left-hand side of the device and the etched wire (via an Al contact pad) on the right-hand side of the device. The position of the formed tunnel barrier is indicated in red. The magnetic field axes relative to the device are also shown, and (c) the heterostructure stack. The electrostatic gates – gold colour, the aluminium – light grey and the InAs mesa – dark grey throughout.

Here, we make use of tunnelling conductance spectroscopy to probe the above-gap regime of a quasi-1D nanowire, formed via the subtractive etching of a superconducting-semiconducting Al-InAs heterostructure. Although tunnel spectroscopy has been widely used for probing the sub-gap structure and identifying low-

* james.witt@sydney.edu.au

† david.reilly@sydney.edu.au

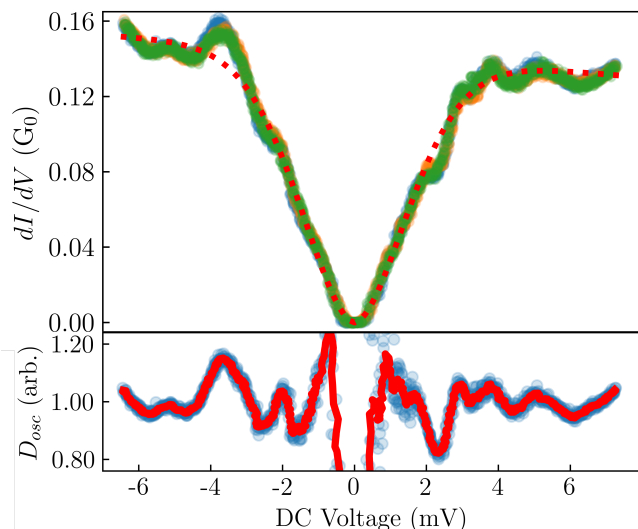


FIG. 2. Upper panel: the measured differential conductance, dI/dV , as a function of bias at zero magnetic field (after x- [green], y- [yellow] and z-axis [blue] magnetic field sweeps). The red dotted line is a fit to the data described in the text. Lower panel: The blue circles are the oscillating part of the ‘wire’ DOS, D_{osc} , extracted from the differential conductance as described in the text (red line) smoothed data.

lying bound states of proximitized hybrid devices [3–10, 19], the regime above the superconducting gap has received less attention. In this regime we observe oscillations in the tunnel conductance which we believe arise from the influence of the 1D sub-bands of the etched quasi-1D InAs wire itself. Fitting a numerical model [25] supports this hypothesis and reveals the strength of the SOI in the confined 1D region – a key parameter in evaluating the suitability of these systems for supporting Majorana bound states.

II. METHODS

The InAs-Al hybrid heterostructure is grown by molecular beam epitaxy using ultra-high purity techniques [26]. The structure includes a complex quantum well of InAs and $\text{In}_{0.90}\text{Ga}_{0.10}\text{As}$ grown on a lower barrier of $\text{In}_{0.81}\text{Al}_{0.19}\text{As}$. A 7 nm Al layer is deposited in-situ after a 2ML GaAs etch stop is deposited on the semiconductor structure. The tunnelling device, along with conventional Hall bar devices, were fabricated using a conventional e-beam lithography process, a phosphoric acid etch to define the mesa and a Transene etch to remove the aluminium layer from the 1D wire part of the device and from the active area of the Hall bars. Patterned and etched samples were then cleaned using the pulse-purge function of the ALD tool prior to depositing a dielectric layer and metallic top-gates [24].

A micrograph and schematic of the device are shown in fig. 1 (a) and (b) respectively. It comprises, on the left

hand side, a wide 2DEG mesa with a central, thin patterned Al strip on top, and on the right, a mesa-etched quasi-1D nanowire without Al on top. There is some variation of the wire width along its length, but near the tunnel barrier it is 280 ± 90 nm [27]. On the left, three metallic top-gates can be seen. The outer top-gates serve to deplete the 2DEG in these regions only. The central top-gate – which mirrors approximately the shape of the underlying patterned Al – extends slightly (of order 20 nm) beyond the Al and thereby, when negatively biased, is able to deplete a thin region of the 2DEG (shown schematically in red). This forms a tunnel barrier between the Al side of the device and the quasi-1D nanowire side of the device. Transport measurements are performed using a standard 4-point lock-in technique with a DC offset bias. The sample is mounted in a dilution refrigerator equipped with a vector-magnet, operating at a temperature < 10 mK (electron temperature, $T_e \sim 55$ mK).

III. RESULTS

The device is operated in the tunnelling regime – the top-gate is used exclusively to form the tunnel barrier. At a bias of -3 V the conductance through the device is of order $0.2 G_0$ or less. The side-gates were found to bear little influence on the experiment and were kept at 0 V. The Al superconducting gap is visible at low-bias before the application of the magnetic field and has a value of $\approx 250 \mu\text{eV}$ [see supplementary information]. After the application of the magnetic fields the superconductivity did not recover and throughout this work we treat the Al as a normal 3D metal.

An example of the differential conductance, dI/dV , as a function of bias across the tunnel barrier can be seen in the upper panel of fig. 2. The three different traces represent the zero magnetic field case taken after each axis field sweep – fields were swept to their extreme positive value, to their extreme negative value and back to zero – 1, 1 and 3 T for the x-, y- and z-axes, respectively. The similarity of the traces after each sweep shows the robustness of the band features after changing the bias and the magnetic field.

The current through a tunnel barrier is directly related to the density of electronic states, $D_{L,R}$, on each side by,

$$I \propto \int_{-\infty}^{\infty} T(E) D_L(E + eV) D_R(E) [f(E) - f(E + eV)] dE,$$

where T is the tunneling coefficient and $f(E)$ is the Fermi-Dirac distribution at energy E .

It is our hypothesis that the oscillatory features in the data correspond to the changing accessibility of the individual quasi-1D bands of the wire, that is, the peaks correspond to the (energetically broadened) van Hove singularities associated with the quasi-1D band minima [28].

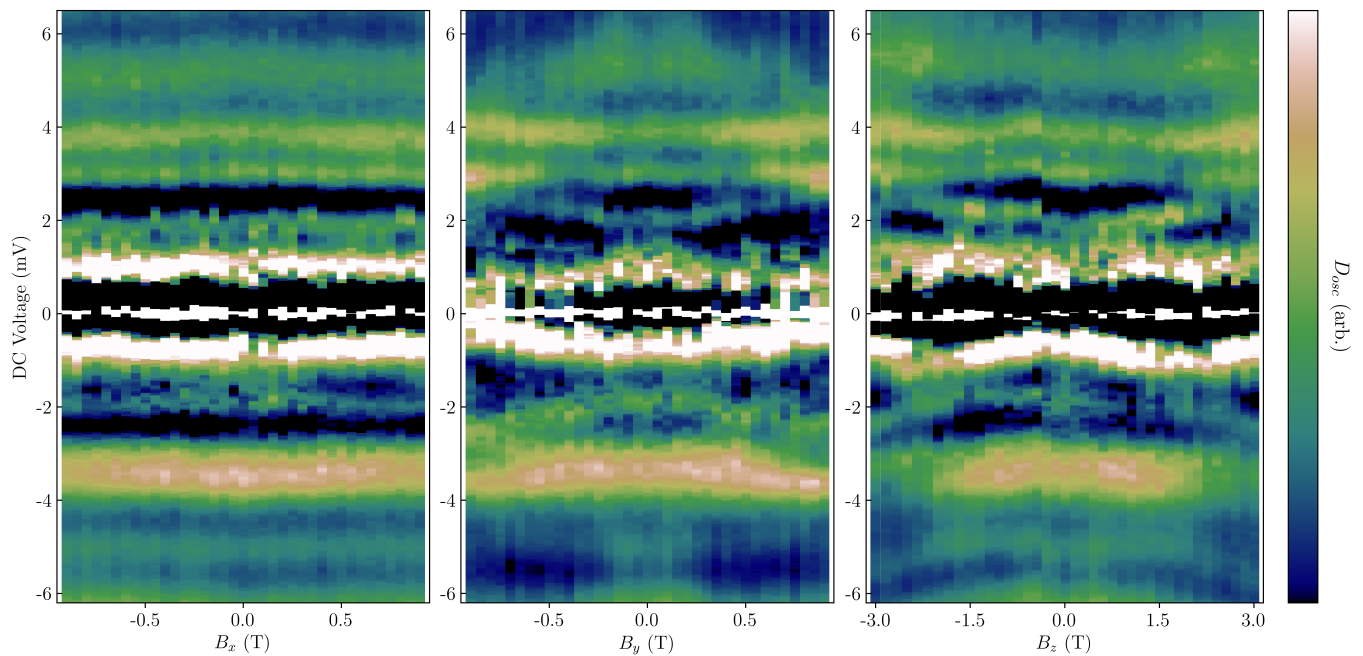


FIG. 3. The magnetic field dependence of the fluctuating part of the measured DOS, D_{osc} , as a function of bias, shown for the three different magnetic field axes. How the axes relate to the device is shown in fig. 1 (b).

The measurement broadened quasi-1D DOS, D_R , can be decomposed into a background term, $D_{bg} \propto \sqrt{E - E_{bm}}$, where E_{bm} is the effective ensemble band minimum, and an oscillating part, D_{osc} (see SI). To isolate the features of interest in the data, D_{osc} , it is necessary to fit the remaining terms of the tunnelling integral, $D_{bg} D_L T(E)$ (a description and justification of the fit is given in the supplementary information)[29–34]. This fit is shown in the upper panel of fig. 2 (red dotted line).

The lower panel of fig. 2 shows D_{osc} (blue circles) extracted from the data in the upper panel. The red curve is a smoothed version which is used throughout the subsequent magnetic field analysis. This method of extracting D_{bg} renders the extracted D_{osc} around zero-bias as undefined – data points between -300 and 300 μeV have therefore been excluded from the analysis.

There is considerable, robust structure to the D_{osc} data. The data display a somewhat periodic modulation with a peak spacing of ~ 1 meV. Although the periodicity of the peak positions in energy is somewhat regular, the magnitudes (occupancy) clearly differ.

Figure 3 shows the fluctuating part of the DOS, D_{osc} , as a function of applied magnetic field along three different axes. As above, the zero bias regime does not offer any meaningful information and has been excluded. The oscillations visible in fig. 2 are much more easily discerned when viewed as a function of magnetic field and there are distinct differences between the different axes. The sub-band structure appears largely insensitive to a magnetic field in the x -axis direction. Band deflection and band splitting, however, are visible for a magnetic field applied in both y - and z -axes (N.B. due to the type

of vector magnet used, the z -axis field range is greater than that of the x - and y -axes).

IV. MODELLING

To model the system, we followed the method of Zhang *et al.* [25] – a numerical perturbative approach which includes the effects of the Rashba and Dresselhaus SOI as well as an SOI arising from the transverse confinement, along with the Zeeman effect. The model treats the transverse confinement (in x) as due to a parabolic potential and considers the application of a magnetic field along the y -axis only.

We calculate the dispersion relation for the different bands, $E(k)_n$, using this model, and then track the band minima as a function of applied magnetic field. These band minima along with the data from the central panel of fig. 3 (now in grey-scale) are shown in fig. 4. The red and blue curves represent the different spin-bands. The solid and dotted lines are directly from the model – the dotted lines show bands (or sections of bands) that do not have an obvious experimental equivalent in the data. The dot-dashed lines have different model parameters, discussed below and have been shifted in energy to better fit the data.

The fit shown was achieved with a Rashba parameter, $\alpha_R = 3.0 \times 10^{-12}$ eVm, the Dresselhaus parameter, $\beta_D = 0$ eVm, and the lateral spin-orbit parameter, $\gamma = 5.0 \times 10^{-13}$ eVm. The model was found to be largely insensitive to the g -factor in this field regime over the

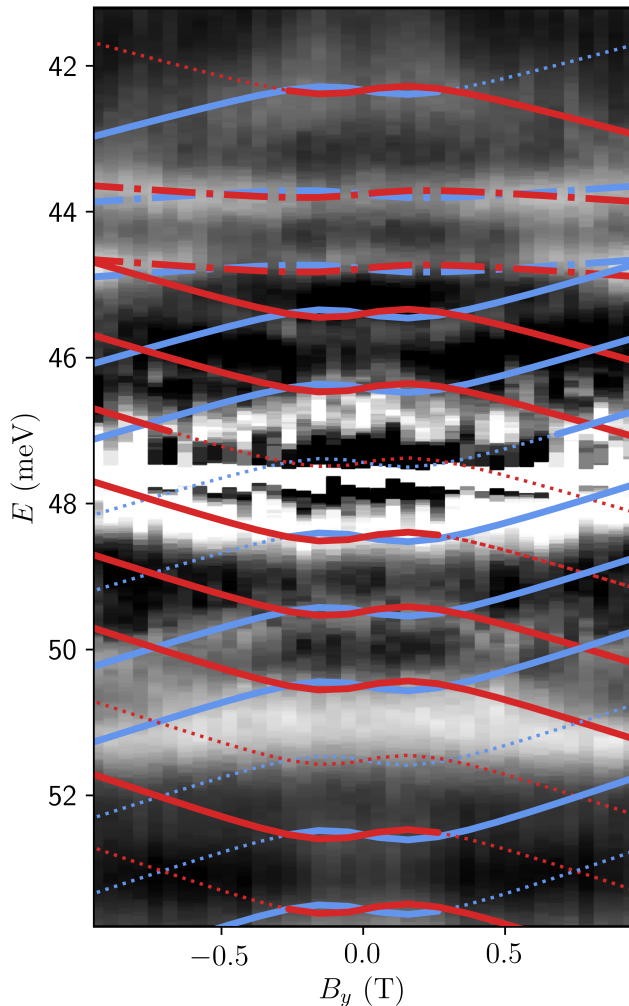


FIG. 4. The magnetic field dependence of the fluctuating part of the measured DOS, D_{osc} , as a function of bias, E (meV), for magnetic field in the y -axis direction. The energy is relative to the ensemble band minimum, E_{bm} . The red and blue lines are the different spin species of the modelled 1D sub-band structure. The solid lines are fits to the data, the dotted lines are band edges predicted by the model which have no obvious experimentally observed counterpart and the dot-dashed lines are fits which required modified fitting parameters.

range of realistic values considered [35], as such, it was maintained at $g = 17$. With reference to the simple 1D DOS approximation (discussed in the SI) we considered the band number, n , to be centered about 48 (although due to the regular spacing of the bands, this choice is not critical to the analysis). The lateral confining potential is characterised by an angular frequency which we set as $\omega_0 = 1.55 \times 10^{12}$ Hz in order to achieve a level spacing comparable to that measured experimentally. This frequency corresponds to a length-scale, $l_0 \sim 50$ nm, which is of the order of the wire width, which is 280 ± 90 nm as measured (although the 2DEG itself will be confined to a narrower region due to disorder at the wire edge). To

fit the dot-dashed curves, the Rashba term was reduced to $\alpha_R = 2.0 \times 10^{-12}$ eVm and the transverse SOI term to $\gamma = 2.0 \times 10^{-13}$ eVm, whilst everything else was kept as before.

V. DISCUSSION

The model is able to reproduce the key features and dependencies present in the data with a very reasonable value for the x -axis parabolic confining potential. From measurements performed on comparable samples, α_R and β_D are also reasonable and consistent for this type of stack [36–38]. The lateral spin-orbit parameter, γ , is somewhat of an unknown quantity, but could reasonably be assumed to be of a similar order as the Rashba coupling parameter – here we see it an order of magnitude smaller.

There are also, however, some irregularities across the measured range not accounted for by the model and it is apparent that several of the bands appear much more strongly in one spin or one directional splitting. There is also an apparently absent band (the third from the bottom) which seems possibly to be shifted into the adjacent band – the brightest feature across this region. These inconsistencies suggest that there are possible additional terms that couple different bands which are not captured by this model. The reduction of the SOI and shifting in energy of only very specific and localised (in energy) bands at such a high band number, n , strongly suggests something akin to donor levels arising from impurities and coupling to bands at specific energies. It is also a possibility that non-parabolicity could account for this, although the regular spacing away from these shifted levels makes this an unlikely explanation.

VI. CONCLUSION

In conclusion, we have demonstrated the feasibility of fabricating, using a subtractive process, a device possessed of quasi-1D characteristics and have shown the magnetic field dependence thereof. We were able to fit the data in one of the magnetic field directions with energy and SOI values that are consistent with the geometry of the device and the materials employed. Having shown that the 1D modes in a confined 2DEG are evenly spaced in energy, in principle, this allows one to address or occupy specific states of interest more easily and reliably than the mode structure of grown nanowires, which can be complex and highly degenerate. With the addition of an electrostatic gate to this system – to adjust the energy of the bands in the mesa-etched 1D wire – it is likely possible to move the wire from an even number of occupied bands to an odd number – an essential ingredient for MBS generation. In addition, this technique also allows for the extraction of the strength of the SOI coupling parameters of a 1D system.

VII. ACKNOWLEDGEMENTS

We wish to thank S. Pauka, A. Jouan, and M. Casidy for useful conversations and technical help. This research was supported by the Microsoft Corporation and

the Australian Research Council Centre of Excellence for Engineered Quantum Systems (EQUS, CE170100009). The authors acknowledge the facilities as well as the scientific and technical assistance of the Research & Prototype Foundry Core Research Facility at the University of Sydney, part of the Australian National Fabrication Facility.

-
- [1] R. Lutchyn, E. P. A. M. Bakkers, L. P. Kouwenhoven, P. Krogstrup, C. M. Marcus, and Y. Oreg. Majorana zero modes in superconductor–semiconductor heterostructure. *Nat. Rev. Mater.*, 3:52, 2018. doi: <https://doi.org/10.1038/s41578-018-0003-1>.
- [2] S. M. Frolov, M. J. Manfra, and J. D. Sau. Topological superconductivity in hybrid devices. *Nature Physics*, 16(7):718–724, Jul 2020. doi:10.1038/s41567-020-0925-6.
- [3] V. Mourik, K. Zuo, S. M. Frolov, S. R. Plissard, E. P. A. M. Bakkers, and L. P. Kouwenhoven. Signatures of majorana fermions in hybrid superconductor–semiconductor nanowire devices. *Science*, 336(6084):1003–1007, 2012. doi:10.1126/science.1222360.
- [4] M. T. Deng, C. L. Yu, G. Y. Huang, M. Larsson, P. Caroff, and H. Q. Xu. Anomalous zero-bias conductance peak in a nb–insb nanowire–nb hybrid device. *Nano Letters*, 12(12):6414–6419, 2012. doi:10.1021/nl303758w.
- [5] Anindya Das, Yuval Ronen, Yonatan Most, Yuval Oreg, Moty Heiblum, and Hadas Shtrikman. Zero-bias peaks and splitting in an al–inas nanowire topological superconductor as a signature of majorana fermions. *Nature Physics*, 8(12):887–895, Dec 2012. doi:10.1038/nphys2479.
- [6] H. O. H. Churchill, V. Fatemi, K. Grove-Rasmussen, M. T. Deng, P. Caroff, H. Q. Xu, and C. M. Marcus. Superconductor–nanowire devices from tunneling to the multichannel regime: Zero-bias oscillations and magnetoconductance crossover. *Phys. Rev. B*, 87:241401, Jun 2013. doi:10.1103/PhysRevB.87.241401.
- [7] A. D. K. Finck, D. J. Van Harlingen, P. K. Mohseni, K. Jung, and X. Li. Anomalous modulation of a zero-bias peak in a hybrid nanowire–superconductor device. *Phys. Rev. Lett.*, 110:126406, Mar 2013. doi:10.1103/PhysRevLett.110.126406. URL <https://link.aps.org/doi/10.1103/PhysRevLett.110.126406>.
- [8] M. T. Deng, S. Vaitiekėnas, E. B. Hansen, J. Danon, M. Leijnse, K. Flensberg, J. Nygård, P. Krogstrup, and C. M. Marcus. Majorana bound state in a coupled quantum-dot hybrid–nanowire system. *Science*, 354(6319):1557–1562, 2016. doi:10.1126/science.aaf3961.
- [9] Jun Chen, Peng Yu, John Stenger, Moira Hocoavar, Diana Car, Sébastien R. Plissard, Erik P. A. M. Bakkers, Tudor D. Stanescu, and Sergey M. Frolov. Experimental phase diagram of zero-bias conductance peaks in superconductor/semiconductor nanowire devices. *Science Advances*, 3(9), 2017. doi:10.1126/sciadv.1701476.
- [10] Önder Gül, Hao Zhang, Jouri D. S. Bommer, Michiel W. A. de Moor, Diana Car, Sébastien R. Plissard, Erik P. A. M. Bakkers, Attila Geresdi, Kenji Watanabe, Takashi Taniguchi, and Leo P. Kouwenhoven. Ballistic majorana nanowire devices. *Nature Nanotechnology*, 13(3):192–197, Mar 2018. doi:10.1038/s41565-017-0032-8.
- [11] Joon Sue Lee, Sukgeun Choi, Mihir Pendharkar, Daniel J. Pennachio, Brian Markman, Michael Seas, Sebastian Koelling, Marcel A. Verheijen, Lucas Casparis, Karl D. Petersson, Ivana Petkovic, Vanessa Schaller, Mark J. W. Rodwell, Charles M. Marcus, Peter Krogstrup, Leo P. Kouwenhoven, Erik P. A. M. Bakkers, and Chris J. Palmstrøm. Selective-area chemical beam epitaxy of in-plane inas one-dimensional channels grown on inp(001), inp(111)b, and inp(011) surfaces. *Phys. Rev. Materials*, 3:084606, Aug 2019. doi:10.1103/PhysRevMaterials.3.084606. URL <https://link.aps.org/doi/10.1103/PhysRevMaterials.3.084606>.
- [12] S. Vaitiekėnas, A. M. Whiticar, M.-T. Deng, F. Krizek, J. E. Sestoft, C. J. Palmstrøm, S. Marti-Sanchez, J. Arbiol, P. Krogstrup, L. Casparis, and C. M. Marcus. Selective-area-grown semiconductor–superconductor hybrids: A basis for topological networks. *Phys. Rev. Lett.*, 121:147701, Oct 2018. doi:10.1103/PhysRevLett.121.147701. URL <https://link.aps.org/doi/10.1103/PhysRevLett.121.147701>.
- [13] Roy L. M. Op het Veld, Di Xu, Vanessa Schaller, Marcel A. Verheijen, Stan M. E. Peters, Jason Jung, Chuyao Tong, Qingzhen Wang, Michiel W. A. de Moor, Bart Hesselmann, Kiefer Vermeulen, Jouri D. S. Bommer, Joon Sue Lee, Andrey Sarikov, Mihir Pendharkar, Anna Marzegalli, Sebastian Koelling, Leo P. Kouwenhoven, Leo Miglio, Chris J. Palmstrøm, Hao Zhang, and Erik P. A. M. Bakkers. In-plane selective area insb–al nanowire quantum networks. *Communications Physics*, 3(1):59, Mar 2020. ISSN 2399-3650. doi:10.1038/s42005-020-0324-4. URL <https://doi.org/10.1038/s42005-020-0324-4>.
- [14] Pavel Aseev, Alexandra Fursina, Frenk Boekhout, Filip Krizek, Joachim E. Sestoft, Francesco Borsoi, Sebastian Heedt, Guanzhong Wang, Luca Binci, Sara Martí-Sánchez, Timm Swoboda, René Koops, Emanuele Uccelli, Jordi Arbiol, Peter Krogstrup, Leo P. Kouwenhoven, and Philippe Caroff. Selectivity map for molecular beam epitaxy of advanced iii–v quantum nanowire networks. *Nano Letters*, 19(1):218–227, Jan 2019. ISSN 1530-6984. doi:10.1021/acs.nanolett.8b03733. URL <https://doi.org/10.1021/acs.nanolett.8b03733>.
- [15] Pavel Aseev, Guanzhong Wang, Luca Binci, Amrita Singh, Sara Martí-Sánchez, Marc Botifoll, Lieuwe J. Stek, Alberto Bordin, John D. Watson, Frenk Boekhout, Daniel Abel, John Gamble, Kevin Van Hoogdalem, Jordi Arbiol, Leo P. Kouwenhoven, Gijs de Lange, and Philippe Caroff. Ballistic insb nanowires and networks via metal-sown selective area growth. *Nano Letters*, 19(12):9102–9111, Dec 2019. ISSN 1530-6984. doi:10.1021/acs.nanolett.9b04265. URL <https://doi.org/10.1021/acs.nanolett.9b04265>.

- 10.1021/acs.nanolett.9b04265.
- [16] L Desplanque, A Bucamp, D Troadec, G Patriarche, and X Wallart. In-plane InSb nanowires grown by selective area molecular beam epitaxy on semi-insulating substrate. *Nanotechnology*, 29(30):305705, may 2018. doi:10.1088/1361-6528/aac321. URL <https://doi.org/10.1088/1361-6528/aac321>.
- [17] M. Kjaergaard, F. Nichele, H. J. Suominen, M. P. Nowak, M. Wimmer, A. R. Akhmerov, J. A. Folk, K. Flensberg, J. Shabani, C. J. Palmström, and C. M. Marcus. Quantized conductance doubling and hard gap in a two-dimensional semiconductor–superconductor heterostructure. *Nature Communications*, 7(1):12841, Sep 2016. ISSN 2041-1723. doi:10.1038/ncomms12841. URL <https://doi.org/10.1038/ncomms12841>.
- [18] J. Shabani, M. Kjaergaard, H. J. Suominen, Younghyun Kim, F. Nichele, K. Pakrouski, T. Stankevic, R. M. Lutchyn, P. Krogstrup, R. Feidenhans'l, S. Kraemer, C. Nayak, M. Troyer, C. M. Marcus, and C. J. Palmström. Two-dimensional epitaxial superconductor-semiconductor heterostructures: A platform for topological superconducting networks. *Phys. Rev. B*, 93:155402, Apr 2016. doi:10.1103/PhysRevB.93.155402. URL <https://link.aps.org/doi/10.1103/PhysRevB.93.155402>.
- [19] Fabrizio Nichele, Asbjørn C. C. Drachmann, Alexander M. Whiticar, Eoin C. T. O’Farrell, Henri J. Suominen, Antonio Fornieri, Tian Wang, Geoffrey C. Gardner, Candice Thomas, Anthony T. Hatke, Peter Krogstrup, Michael J. Manfra, Karsten Flensberg, and Charles M. Marcus. Scaling of majorana zero-bias conductance peaks. *Phys. Rev. Lett.*, 119:136803, Sep 2017. doi:10.1103/PhysRevLett.119.136803.
- [20] H. J. Suominen, M. Kjaergaard, A. R. Hamilton, J. Shabani, C. J. Palmström, C. M. Marcus, and F. Nichele. Zero-energy modes from coalescing andreev states in a two-dimensional semiconductor-superconductor hybrid platform. *Phys. Rev. Lett.*, 119:176805, Oct 2017. doi:10.1103/PhysRevLett.119.176805. URL <https://link.aps.org/doi/10.1103/PhysRevLett.119.176805>.
- [21] Sébastien R. Plissard, Dorris R. Slapak, Marcel A. Verheijen, Moïra Hoeschele, George W. G. Immink, Ilse van Weperen, Stevan Nadj-Perge, Sergey M. Frolov, Leo P. Kouwenhoven, and Erik P. A. M. Bakkers. From insb nanowires to nanocubes: Looking for the sweet spot. *Nano Letters*, 12(4):1794–1798, Apr 2012. ISSN 1530-6984. doi:10.1021/nl203846g. URL <https://doi.org/10.1021/nl203846g>.
- [22] Diana Car, Jia Wang, Marcel A. Verheijen, Erik P. A. M. Bakkers, and Sébastien R. Plissard. Rationally designed single-crystalline nanowire networks. *Advanced Materials*, 26(28):4875–4879, 2014. doi:<https://doi.org/10.1002/adma.201400924>. URL <https://onlinelibrary.wiley.com/doi/abs/10.1002/adma.201400924>.
- [23] A. T. Hatke, T. Wang, C. Thomas, G. C. Gardner, and M. J. Manfra. Mobility in excess of $10^6\text{cm}^2/\text{V s}$ in inas quantum wells grown on lattice mismatched inp substrates. *Applied Physics Letters*, 111(14):142106, 2017. doi:10.1063/1.4993784.
- [24] S. J. Pauka, J. D. S. Witt, C. N. Allen, B. Harlech-Jones, A. Jouan, G. C. Gardner, S. Gronin, T. Wang, C. Thomas, M. J. Manfra, J. Gukelberger, J. Gamble, D. J. Reilly, and M. C. Cassidy. Repairing the surface of inas-based topological heterostructures. *Journal of Applied Physics*, 128:114301, 2020. doi:<https://doi.org/10.1063/5.0014361>.
- [25] Tong-Yi Zhang, Wei Zhao, and Xue-Ming Liu. Energy dispersion of the electrosubbands in parabolic confining quantum wires: interplay of rashba, dresselhaus, lateral spin–orbit interaction and the zeeman effect. *J. Phys.: Condens. Matter*, 21:335501, 2009. doi:10.1088/0953-8984/21/33/335501.
- [26] G. C. Gardner, S. Fallahi, J. D. Watson, and M. J. Manfra. Modified mbe hardware and techniques and role of gallium purity for attainment of two dimensional electron gas mobility $> 35 \times 10^6\text{cm}^2/\text{Vs}$ in algaas/gaas quantum wells grown by mbe. *Journal of Crystal Growth*, 441:71 – 77, 2016. ISSN 0022-0248. doi:<https://doi.org/10.1016/j.jcrysgro.2016.02.010>.
- [27] Note1. It should also be noted that the measured visual width of the wire will exceed that of the 2DEG formed within – from etch induced disorder and the confining potential.
- [28] C. C. Eugster, J. A. del Alamo, M. J. Rooks, and M. R. Melloch. One-dimensional to one-dimensional tunnelling between electron waveguides. *Applied Physics Letters*, 64(23):3157–3159, 1994. doi:10.1063/1.111324. URL <https://doi.org/10.1063/1.111324>.
- [29] M. H. Devoret, D. Esteve, H. Grabert, G.-L. Ingold, H. Pothier, and C. Urbina. Effect of the electromagnetic environment on the coulomb blockade in ultrasmall tunnel junctions. *Phys. Rev. Lett.*, 64:1824–1827, Apr 1990. doi:10.1103/PhysRevLett.64.1824. URL <https://link.aps.org/doi/10.1103/PhysRevLett.64.1824>.
- [30] Hermann Grabert and Michel H. Devoret, editors. *Single Charge Tunneling: Coulomb Blockade Phenomena In Nanostructures*. Springer, Boston, MA, 1992. doi:<https://doi.org/10.1007/978-1-4757-2166-9>.
- [31] Vladimir A. Ukraintsev. Data evaluation technique for electron-tunneling spectroscopy. *Phys. Rev. B*, 53:11176–11185, Apr 1996. doi:10.1103/PhysRevB.53.11176. URL <https://link.aps.org/doi/10.1103/PhysRevB.53.11176>.
- [32] E. B. Sonin. Tunneling into 1d and quasi-1d conductors and luttinger-liquid behavior. *Journal of Low Temperature Physics*, 124(1):321–334, Jul 2001. ISSN 1573-7357. doi:10.1023/A:1017598423240. URL <https://doi.org/10.1023/A:1017598423240>.
- [33] R. Tarkiainen, M. Ahlskog, J. Penttilä, L. Roschier, P. Hakonen, M. Paalanen, and E. Sonin. Multi-walled carbon nanotube: Luttinger versus fermi liquid. *Phys. Rev. B*, 64:195412, Oct 2001. doi:10.1103/PhysRevB.64.195412. URL <https://link.aps.org/doi/10.1103/PhysRevB.64.195412>.
- [34] Lutz Waldecker, Roman Bertoni, Ralph Ernstorfer, and Jan Vorberger. Electron-phonon coupling and energy flow in a simple metal beyond the two-temperature approximation. *Phys. Rev. X*, 6:021003, Apr 2016. doi:10.1103/PhysRevX.6.021003. URL <https://link.aps.org/doi/10.1103/PhysRevX.6.021003>.
- [35] Joon Sue Lee, Borzoyeh Shojaei, Mihir Pendharkar, Anthony P. McFadden, Younghyun Kim, Henri J. Suominen, Morten Kjaergaard, Fabrizio Nichele, Hao Zhang, Charles M. Marcus, and Chris J. Palmström. Transport studies of epi-al/inas two-dimensional electron gas systems for required building-blocks in topological superconductor networks. *Nano Letters*, 19(5):3083–3090,

2019. doi:10.1021/acs.nanolett.9b00494.
- [36] J. P. Heida, B. J. van Wees, J. J. Kuipers, T. M. Klapwijk, and G. Borghs. Spin-orbit interaction in a two-dimensional electron gas in a *inas/alsb* quantum well with gate-controlled electron density. *Phys. Rev. B*, 57:11911–11914, May 1998. doi:10.1103/PhysRevB.57.11911. URL <https://link.aps.org/doi/10.1103/PhysRevB.57.11911>.
- [37] B. Shojaei, P. J. J. O'Malley, J. Shabani, P. Roushan, B. D. Schultz, R. M. Lutchyn, C. Nayak, J. M. Martinis, and C. J. Palmström. Demonstration of gate control of spin splitting in a high-mobility *inas/alsb* two-dimensional electron gas. *Phys. Rev. B*, 93:075302, Feb 2016. doi:10.1103/PhysRevB.93.075302. URL <https://link.aps.org/doi/10.1103/PhysRevB.93.075302>.
- [38] Kaushini S. Wickramasinghe, William Mayer, Joseph Yuan, Tri Nguyen, Lucy Jiao, Vladimir Manucharyan, and Javad Shabani. Transport properties of near surface *inas* two-dimensional heterostructures. *Appl. Phys. Lett.*, 113:262104, 2018.

Supplementary Information: Spin-orbit Energies in Etch-Confined Superconductor-Semiconductor Nanowires

J. D. S. Witt,^{1,*} G. C. Gardner,^{2,3} C. Thomas,^{2,3} T. Lindemann,^{2,3}

S. Gronin,^{2,3} M. J. Manfra,^{2,3} and D. J. Reilly^{1,4,†}

¹*ARC Centre of Excellence for Engineered Quantum Systems,
School of Physics, The University of Sydney, Sydney, NSW 2006, Australia*

²*Department of Physics and Astronomy,
Purdue University, West Lafayette, Indiana, USA*

³*Microsoft Quantum Purdue, Purdue University, West Lafayette, Indiana, USA*

⁴*Microsoft Quantum Sydney, The University of Sydney, Sydney, NSW 2006, Australia*

(Dated: November 25, 2021)

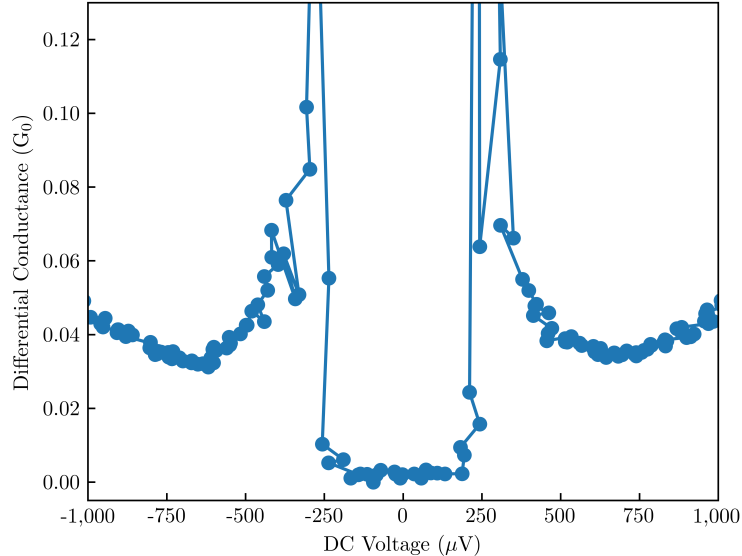


FIG. 1.

I. HALL MEASUREMENTS

From the (top-gated) Hall bar, patterned on the same chip, the electron density was found to be between $0.5 - 2.5 \times 10^{12} \text{ cm}^{-2}$ with a mobility of between $3,000 - 7,000 \text{ cm}^2\text{V}^{-1}\text{s}^{-1}$.

II. SUPERCONDUCTING GAP

Figure 1 shows the superconducting gap in the low-bias regime. The values of the gap, $\Delta \sim 250 \mu\text{eV}$.

III. 1D DOS APPROXIMATION

Figure 2 (left) shows the simulated ideal quasi-1D DOS (black line) for an idealised parabolic potential, equivalent to equally spaced bands with individual $1\text{D DOS} \propto 1/\sqrt{E}$. The overall trend can be well approximated by, $D_{bg} \propto \sqrt{E - E_{bm}}$ (red line). The irregularity in the height of the Van Hove singularities is an artefact of the plot resolution. The band ensemble minimum, $E_{bm} = 48 \text{ meV}$, for a discussion of this value see section IV.

* james.witt@sydney.edu.au

† david.reilly@sydney.edu.au

The thermal broadening in our system is only $\approx 5 \mu\text{eV}$, the smoothing of the features that we observe most likely arises from a combination of this and the lock-in excitation $\approx 100 \mu\text{eV}$.

Figure 2 (right) shows an expanded section of the left panel around the Fermi energy. A simulated $D_{bg} + D_{osc}$, where $D_{osc} \propto |\sin(\lambda_V)|$, is shown as an example of broadening (green line).

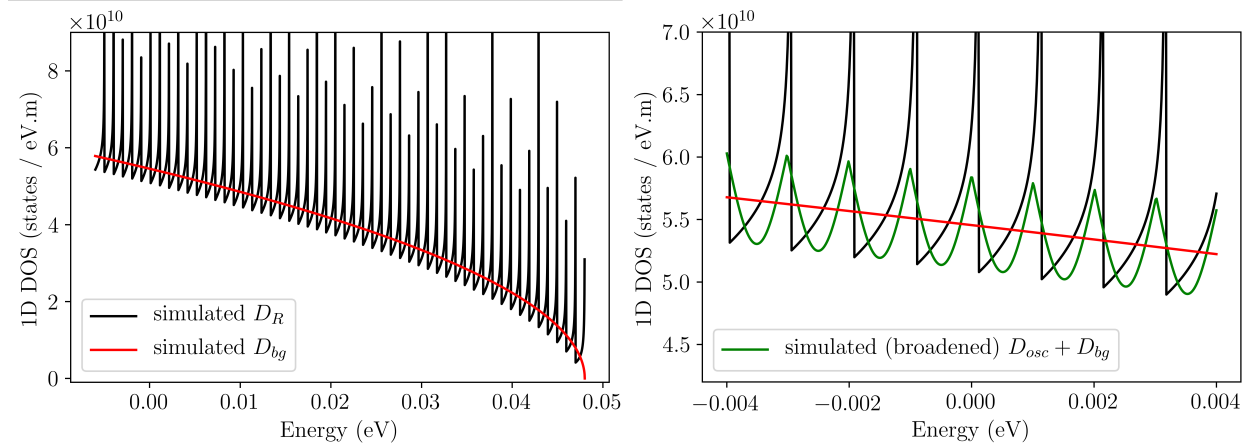


FIG. 2.

IV. 2D \rightarrow QUASI-1D

The band minimum in the quasi-1D DOS approximation is set so that the total electron number calculated from the occupation of the 1D bands up to the Fermi energy is consistent with the measured 2D electron density when approaching the quasi-1D limit. Considering the errors in wire width and measured 2D electron density, the band minimum, $E_{bm} = 48 \pm 13 \text{ meV}$.

V. FITTING $D_{bg}D_L T(E)$

To isolate the oscillatory features in the data which arise from the peaked DOS at the quasi-1D band minima, D_{osc} , it is necessary to fit the other terms in the tunnelling relation. The form used for D_{bg} is given above and is shown in fig. 3 (with a change of units) along with D_L – considered as arising from an ideal 3D metal with a Fermi energy of 11.6 eV – for

Al this is a reasonable assumption [?]. It should be noted that the percentage change of states over the applicable energy range (shown) is much more significant for the wire than for the 3D metal. Hence, although the wire DOS is much lower, it has an appreciable effect on the tunnelling conductance.

The actual conductance will be scaled by the number of atomic sites participating in the tunnelling in conjunction with the transmission coefficient, $T(E)$, which also defines the characteristic tunneling conductance shape.

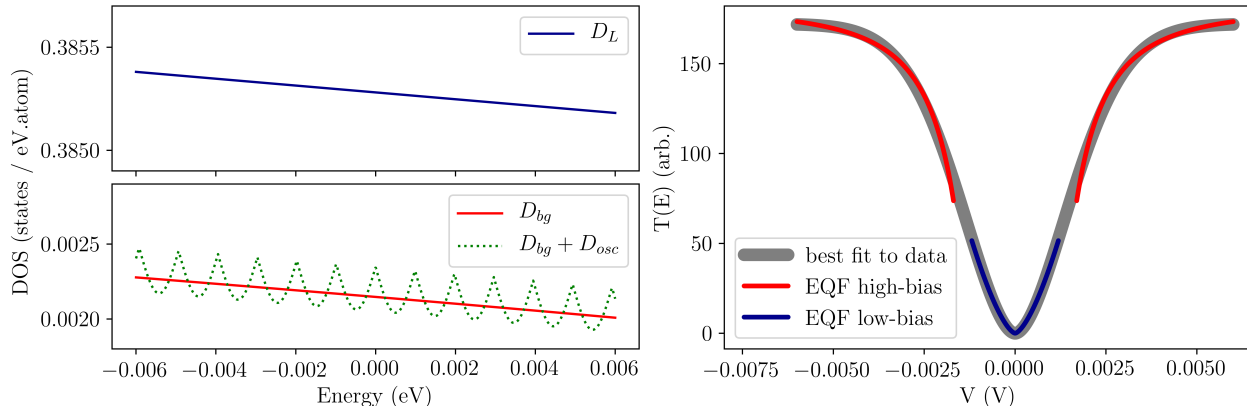


FIG. 3.

To describe the transmission coefficient in tunnelling from a 3D metal to a quasi-1D system the Environment Quantum Fluctuation (EQF) theory should be used [? ? ? ?]. At low-bias – when the voltage, $V < e/C_T$, where C_T is the tunnel junction capacitance – the model describes the *Coloumb blockade* regime. In this regime the differential conductance has a power-law dependence on voltage,

$$\frac{dI}{dV} \propto V^{\alpha_E}$$

where $\alpha_E = 2Z/R_K$, Z is the impedance of the circuit environment, and $R_K = 25,813 \Omega$ is the von Klitzing constant. It should be noted that in this analysis all of the DOS terms are absorbed into the constant of proportionality, what remains is a combination of $T(E)$ and the distribution functions. These terms are grouped under the $T(E)$ term here. From fitting the data in this regime (blue curve in the right panel of fig. 3), $\alpha = 1.5$, giving $Z = 19.4 \text{ k}\Omega$.

In the high-bias regime, the differential conductance is described by,

$$\frac{dI}{dV} = \frac{1}{R_T} - \frac{2}{\alpha_E R_T} \left(\frac{e}{2\pi C_T} \right)^2 \frac{1}{V^2}$$

where R_T is the junction resistance (by fitting $T(E)$ instead of dI/dV , R_T serves as a scaling parameter). Using α_E from the fit to the low-bias regime, it is possible to fit the data (red curve in the right panel of fig. 3) and extract a value of $C_T = 23$ aF. Assuming the tunnel barrier area is defined by the wire width and the well depth, the value of C_T extracted, yields a reasonable tunnel barrier thickness, $t_B = 8.5$ nm.

The black curve in the right panel of fig. 3 shows an approximation of these fitting functions which bridges the two regimes and was used in the analysis in the main paper to extract the varying values of D_{osc} .

VI. ALTERATIONS TO ZHANG *ET AL.*

N.B. Our axis labelling differs from Zhang – z and y are interchanged in our treatment. The Rashba term, $(H_R)_{nn}^{\pm\mp}$ (eqn 22) in our model has a sign change for the different spin species. We explicitly calculate the expansion coefficients, $a_{n,\sigma}$, from perturbation theory and then calculate the perturbed eigenvalues, E_ϕ , as a function of k . We have reduced the ‘flattening’ field dependence aspect of the unperturbed eigen-energies which we believe to be equivalent to inserting a chemical potential term, μ , to maintain total charge number.